

The capture of halo material by orbiting subhaloes

Hang Yang,^{1,3,4*} Simon D.M. White,² and Liang Gao^{1,3,4}

¹ *Institute for Frontiers in Astronomy and Astrophysics, Beijing Normal University, Beijing 102206, China*

² *Max Planck Institute for Astrophysics, Karl-Schwarzschild-Strasse 1, 85740 Garching, Germany*

³ *School of Physics and Astronomy, Beijing Normal University, Beijing 100875, China*

⁴ *Institute for Astrophysics, School of Physics, Zhengzhou University, Zhengzhou 450001, China*

Accepted XXX. Received YYY; in original form ZZZ

ABSTRACT

When a dark matter halo falls into a more massive object and becomes a subhalo, it typically loses much of its mass through tidal stripping. The reverse process is also possible in principle. The subhalo may gravitationally capture material from its host. If sufficiently efficient, this process could make an initially starless subhalo visible. We use high-resolution N-body simulations to estimate the efficiency of capture. We find that after an extended period orbiting within its host, at most $\sim 10^{-4}$ of a subhalo's remaining mass has been acquired since infall. This captured material is less concentrated to subhalo centre than material retained from before infall. It is also very much less abundant than host material that is instantaneously passing through the subhalo on almost unperturbed orbits. Captured stars are not sufficiently spatially concentrated to be distinguished from the dominant background of "field" stars, and their concentration in velocity space is no greater than that of typical stellar streams in the halo. Unfortunately, stellar capture is not efficient enough to allow initially starless low-mass subhaloes to be detected.

Key words: methods: numerical – galaxies: evolution – Cosmology: dark matter.

1 INTRODUCTION

In the standard Λ -cold dark matter (Λ CDM) paradigm, cosmic structure grows hierarchically. Small dark matter haloes collapse and come to equilibrium first, thereafter growing in mass by smooth accretion and by merging with other haloes. During this process, accreted haloes are not fully disrupted within their new and more massive hosts; rather their inner regions survive as self-bound subhaloes orbiting within the larger system (e.g. Moore et al. 1998; Gao et al. 2004; Springel et al. 2008).

The mass of the smallest dark matter halo depends on the nature of the dark matter but, for cold dark matter, is assumed to be much smaller than galactic scale. For example, for weakly interacting massive particles (WIMPs) it is set by the damping scale due to early free-streaming, about $10^{-6}M_{\odot}$ for a rest mass of $100 \text{ GeV}/c^2$ (Bertone et al. 2005). Both analytical models (e.g. Press & Schechter 1974; Bond et al. 1991) and numerical simulations (e.g. Sheth & Tormen 1999; Jenkins et al. 2001; Wang et al. 2020; Zheng et al. 2024) have shown that at low mass the present-day abundance of dark matter haloes in a Λ CDM cosmology increases almost as $dN/dM \propto M^{-2}$. This is much steeper than the observed abundance of galaxies as a function of stellar mass, so most low-mass haloes (and subhaloes) must be without stars (e.g. Klypin et al. 1999; Guo et al. 2010; Sawala et al. 2015).

In hierarchical models like Λ CDM, galaxies form by the cooling and condensation of gas at the centres of the growing population of dark matter haloes (White & Rees 1978). It is generally believed that only haloes capable of efficient atomic cooling can sustain star

formation and so build substantial stellar systems. This requires a virial temperature larger than about 10^4 K . In addition, after reionization ($z < 6$) UV photons prevent gas in low-mass haloes from condensing and forming stars (e.g. Efstathiou 1992; Okamoto et al. 2008; Borrow et al. 2023; Zhu & Gao 2024). Considering gas cooling and photoheating together, there is a lower limit of order $10^9 M_{\odot}$ on the mass of present-day haloes that can host a significant galaxy (e.g. Benitez-Llambay & Frenk 2020; Gutcke et al. 2022). Below we will use the term "starless" (sub)haloes to refer to haloes below this star formation limit and to the subhaloes formed when they accrete onto a larger system.

Recently, Peñarrubia et al. (2024) argued that starless subhaloes may become visible by capturing field stars from the stellar halo of their host. If this mechanism is significant, it could make low-mass subhalo populations detectable, thus confirming their existence and giving important insight into the nature of dark matter. As a result, it is of considerable interest to explore this process directly in order to estimate the capture efficiency. Since the capture process for field stars is identical to that for individual dark matter particles on the same orbit, we can estimate the required efficiency by evaluating the frequency with which dark matter particles are captured by orbiting subhaloes. As we show below, this can be evaluated quite accurately using high-resolution N-body simulations.

The paper is organised as follows. In Section 2 we describe the numerical simulations and our analysis methods. The main results are presented in Section 3, and we summarise and discuss them in Section 4.

* E-mail: hyang@nao.cas.cn

2 METHODS

2.1 The Phoenix Simulations

In this paper, we use the dark-matter-only, zoom-in simulations of the Phoenix suite (Gao et al. 2012) to explore whether field particles in a halo can be captured by subhaloes. The collisionless, gravitational dynamics of dark matter particles and of field stars are identical, so we do not need to identify “stars” explicitly in the simulations and can concentrate instead on the capture of dark matter particles. The Phoenix suite resimulated the evolution of nine galaxy cluster regions selected from the Millennium Simulation (Springel et al. 2005). These resimulations were run using GADGET-3, an updated version of the publicly available GADGET-2 code (Springel et al. 2005), adopting WMAP1 cosmological parameters: $\Omega_m = 0.25$, $\Omega_b = 0.048$, $\Omega_\Lambda = 0.75$, $h = 0.73$, $n_s = 1$ and $\sigma_8 = 0.8$ (Spergel et al. 2003). The Friends-of-Friends (FOF, Davis et al. 1985) and SUBFIND (Springel et al. 2001) algorithms were applied to identify halo and subhalo structures, respectively. The Phoenix simulations were run at several mass resolution levels. Here, we use only the level-2 results, the highest resolution available for all nine haloes. These have mass resolution $\sim 10^6 M_\odot$ which, since the halo virial masses range from $7 \times 10^{14} M_\odot$ to $3 \times 10^{15} M_\odot$, corresponds to approximately 10^8 particles within the virial radius R_{200} of each $z = 0$ halo.¹

Gao et al. (2012) showed explicitly and in detail that the evolution of the Phoenix cluster mass haloes closely resembles a scaled up version of that in the Aquarius suite of Milky-Way mass haloes (Springel et al. 2008). Thus we believe that the results we find below should be applicable to halo star capture in the Milky Way’s halo once all masses are scaled down by a factor of 1000 and all distances and velocities by a factor of 10. We check this point explicitly in the Appendix by repeating some of our analysis for the two highest resolution simulations of one of the Aquarius haloes.

2.2 Sample Selection and Analysis Method

Captured particles will be in, or close to a subhalo and will move with it at late times, but they will not be bound to or otherwise associated with it at the time of its accretion. We use the following procedures to identify all such newly associated subhalo particles in each of our Phoenix simulations

1) We track each surviving $z = 0$ subhalo with at least 100 bound particles back to the latest simulation snapshot in which its progenitor lies outside R_{200} of the host halo. We then define the infall redshift of the subhalo z_{inf} as that of the next stored snapshot, and the subhalo’s bound particle number at infall n_{inf} to be the value found at z_{inf} .

2) We find the latest snapshot, $z_{\text{max}} > z_{\text{inf}}$, for which the subhalo’s progenitor is the main subhalo of its FoF group, and we measure its R_{200} at this time. We then go to the snapshot immediately before z_{inf} and record the IDs of all particles that are within r_{limit} of halo centre in this snapshot, taking $r_{\text{limit}} = 2R_{200}(z_{\text{max}})$. For the i -th $z = 0$ subhalo we denote this set of particles as A_i . Our results below are insensitive to the precise definition of r_{limit} .

3) At $z \approx 0.1$, we record the particle IDs of all particles located within twice the tidal radius, $2r_t$ of the centre of each subhalo. We denote this set of particles as B_i . We approximate the tidal radius of a subhalo of SUBFIND mass M_{sub} using the circular orbit formula,

$$r_t = r \left[\frac{M_{\text{sub}}}{(2 - \partial \ln M / \partial \ln r) M(< r)} \right]^{1/3}, \quad (1)$$

¹ We define the virial radius R_{200} as the radius within which the mean density is 200 times the critical density of the Universe.

where r is the distance from main halo centre and $M(< r)$ is the mass enclosed within r (e.g. Tormen et al. 1998; Springel et al. 2008).

4) We apply the same procedure as in step (3) at $z = 0$ and define the corresponding set of particles as C_i .

5) For the i -th subhalo, the particles in the set $B_i \setminus A_i$ (those in B_i but not in A_i) are defined as newly associated particles at $z = 0.1$. Note that we do not require these particles to be bound to the subhalo so they are a superset of captured particles and include particles which are just “passing through”. Particles that belong to $A_i \cap B_i$ (those in both A_i and B_i) are referred to as retained particles.

6) For each subhalo, we also test whether the sets $B_i \setminus A_i$ and C_i share any elements. Particles that belong to both sets are defined as still associated and can be considered as truly captured particles.

In the following analysis, we drop from consideration a small number of subhaloes which experience a merger after their most recent infall. Such mergers could cause starless subhaloes to acquire stars in the so-called “ghost galaxy” scenario (Wang et al. 2023), but here we focus only on the smooth capture mechanism discussed by Peñarrubia et al. (2024).

3 RESULTS

3.1 An illustrative example

Fig. 1 presents an illustrative example, a randomly selected $z = 0$ subhalo which was accreted at $z_{\text{inf}} = 1.08$. In the left panel, which shows the last snapshot in which this object was outside R_{200} of its host halo, the black solid circle represents r_{limit} for the subhalo’s progenitor. The 41638 particles within the corresponding sphere make up set A as defined in Section 2.2. In the middle panel, the black solid circle represents $2r_t$ for the subhalo at $z = 0.11$, so the 2127 particles within this sphere define set B . Similarly, the black solid circle in the right panel represents $2r_t$ for the subhalo at $z = 0$, so the 2348 particles within this sphere define set C . The red dots in the left panel indicate the 1308 particles that will be considered newly associated at $z = 0.1$, and hence belong to set $B \setminus A$. The red dots in the middle panel show 10% of the particles in set A at $z = 0.1$, while the red dots in the right panel show the 1308 particles in $B \setminus A$ at $z = 0$. None of these is still inside $2r_t$ at this time, so $(B \setminus A) \cap C$ is empty.

As the middle panel shows, most particles associated with the infalling halo (95% of set A) are no longer close to the subhalo at $z = 0.11$, but are strewn around the main halo as a result of tidal disruption and mixing processes. There are indeed 1308 particles that are within $2r_t$ of the subhalo at $z = 0.11$ but were not close to it at infall (the red dots in the left panel). However, as shown by the red dots in the right panel, none of these newly associated particles is still within $2r_t$ at $z = 0$, just ~ 1 Gyr later. Thus none of the newly associated particles was permanently captured by the subhalo.

If the subhalo were able to capture field particles temporarily, these might lead to an excess of newly associated particles within the subhalo relative to the surrounding field. In Fig 2 we test whether such temporary capture is significant by plotting the differential and cumulative density profiles of various particle populations at $z = 0.11$. Black solid lines show the profiles for all particles out to $2r_t$, while the red and cyan solid lines split these into retained and newly associated particles, respectively. The red dashed lines include only particles considered bound to the subhalo by SUBFIND; these are 81% of the retained particles within $2r_t$ but almost 100% of them below $0.5r_t$. Within $2r_t$ newly associated particles outnumber retained particles by a factor of about 1.5, but their relative contribution drops

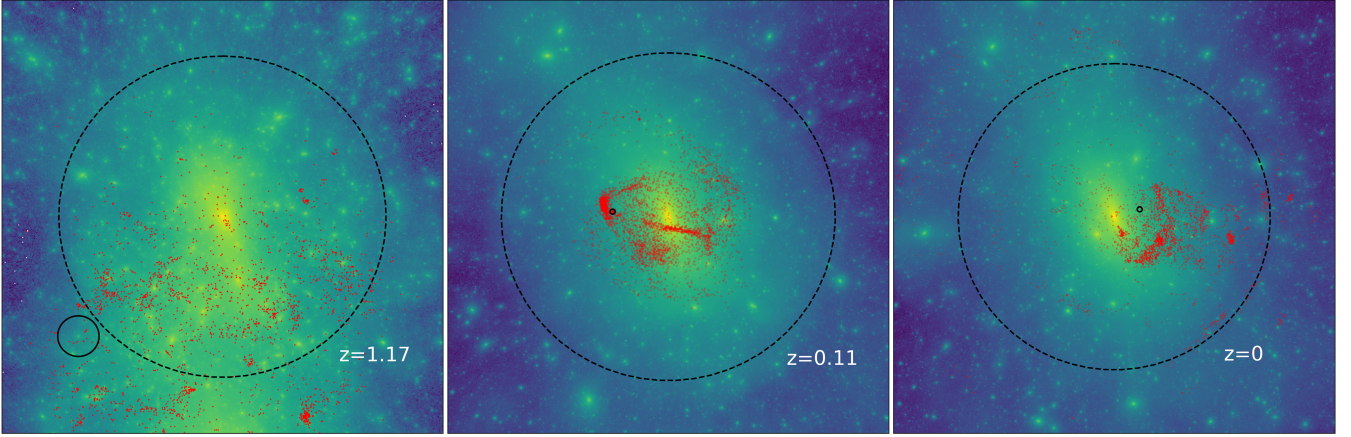


Figure 1. An illustration of our analysis procedure for a randomly selected but relatively massive subhalo with $z_{\text{inf}} = 1.08$. From left to right, the panels show the projected distribution (in comoving coordinates) of mass and of various specific particle sets at $z = 1.17, 0.11$ and 0.0 when sets A, B and C are selected, respectively. The black dashed circles show the virial radius of the main halo in each panel. The solid black circle in the left panel shows r_{limit} for the infalling halo. The red dots in this panel show the 2127 particles that will be considered newly associated to the subhalo at $z = 0.11$. The solid black circles in the middle and right panels indicate $2r_t$ for the subhalo. Red dots in the middle panel show particles that were within r_{limit} in the left panel. For clarity, we display only a random 10% of these 41638 particles; 5% of them are within $2r_t$ at $z = 0.11$. The red dots in the right panel show the $z = 0$ positions of particles that were newly associated at $z = 0.11$ (the same particles plotted in red in the left panel). Each panel is $4\text{cMpc}/h$ on a side.

precipitously at smaller radii. In fact, their space density is everywhere consistent with that of the local field, as is seen most clearly through the close approximation of the cyan line in the right panel to the dashed black line indicating $N(< r) \propto r^3$. These results are consistent with the idea that the subhalo just moves through the field without capturing particles or generating a significant local overdensity. If this were a starless subhalo, it would be very difficult to distinguish captured stars observationally from the background field population.

In Fig. 3, we show the evolution of mass (characterized by SUBFIND bound particle number) and distance from host halo centre for this same subhalo. In both panels the black star indicates t_{inf} while the red star indicates the time when set A was defined. In the right panel, the black dashed line shows the evolution of R_{200} for the host halo. The left panel of Fig. 3 shows that the subhalo has lost 95% of its infall mass by $z = 0$. To characterize the orbit of the subhalo, we estimate the number of pericentric passages N_{orbit} by counting local minima of the blue curve in the right panel; $N_{\text{orbit}} = 6$ in this case.

3.2 Stacked Density Profiles of Subhalos

To obtain representative results based on all subhaloes in our Phoenix resimulations, we stack spherically averaged and normalised density profiles (exactly analogous to Fig. 2) as a function of infall mass and infall redshift for all $z = 0.11$ subhaloes which still have 100 or more bound particles at $z = 0$. We divide these subhaloes into three mass bins according to their bound particle number at infall, $10^2 < n_{\text{inf}} < 10^3$, $10^3 < n_{\text{inf}} < 10^4$ and $10^4 < n_{\text{inf}} < 10^5$.¹ Since most surviving subhaloes were accreted onto their host after $z = 2$ (Gao et al. 2004; Xie & Gao 2015) we here show results only for subhaloes with $z_{\text{inf}} \approx 1$ and $z_{\text{inf}} \approx 2$. For each case, three simulation snapshots close to the chosen redshift were considered.²

The mean density profiles of subhaloes with $z_{\text{inf}} \approx 1$ are shown in

² Specifically, for $z_{\text{inf}} \approx 1$ we used snapshots at $z = 1.08, 0.99$ and 0.91 , while for $z_{\text{inf}} \approx 2$ we used $z = 2.07, 1.91$ and 1.77 .

Fig. 4. Black, red and cyan lines give results for all, for retained and for newly associated particles, respectively. The error bars on the red and cyan curves show the uncertainty in the mean derived from the scatter in the individual values in each bin. The number of subhalo profiles averaged is given as N_{sample} in each panel. In all cases the average result is very similar to that for the individual subhalo shown in Fig. 2; the density of newly associated particles is constant and equal to the surrounding “field” value all the way down to subhalo centre. There is no excess that might be attributed to temporarily or permanently captured particles.

A more direct way to look for newly captured particles is to see if any of the newly associated particles (i.e. the members of $B \setminus A$) is considered bound to the subhalo by SUBFIND. There are indeed a few such particles, but the average ($\langle n_{\text{newly bound}} \rangle$) in the panels of Fig. 4) is fewer than one per subhalo, about 0.01% of the mean bound subhalo mass in all cases with no strong dependence on subhalo mass. Similarly one can check for captured particles independent of SUBFIND by finding the number of newly associated particles at $z \approx 0.1$ which are still associated at $z = 0$ (i.e. particles which are members of $(B \setminus A) \cap C$). The mean number of such particles is given as $\langle n_{\text{still assoc.}} \rangle$ in the panels of Fig. 4, and is again less than one per subhalo, of order 10^{-4} of the subhalo mass.

We also give in Fig. 4, the mean number (N_{orbit}) of orbits completed between z_{inf} and $z \approx 0.1$, and the mean distance of the subhaloes from halo centre at $z \approx 0.1$. Surviving subhaloes with lower n_{inf} (which have on average been reduced in mass by stripping by a smaller factor) have fewer orbits on average and are at larger distances from halo centre.

The stacked profiles for $z_{\text{inf}} \approx 2$ are shown in Fig. 5. These are very similar to those of Fig. 4 and again there is no detected excess of newly associated particles within r_t . Subhaloes with $z_{\text{inf}} \approx 2$ execute more orbits by $z = 0.1$, are closer to halo centre on average, and lose more mass on average than their counterparts with $z_{\text{inf}} \approx 1$. This a natural consequence of the longer time they have spent within their host halo. Despite this longer residence time, the values of $\langle n_{\text{newly bound}} \rangle$ and

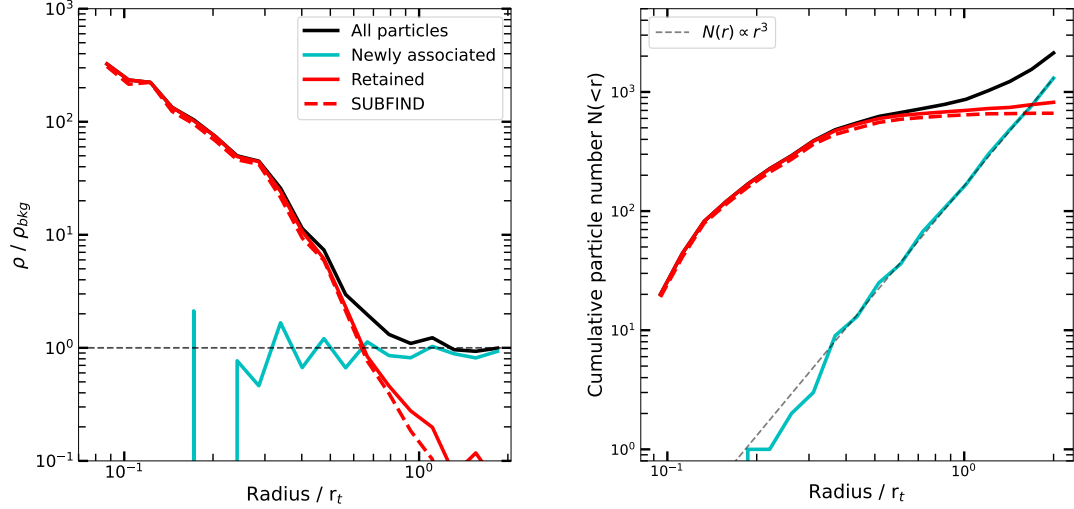


Figure 2. Left panel: Density profiles for the subhalo of Fig.1 at $z = 0.11$ with radius normalised by r_t and density normalised by ρ_{bkg} , the mean density in the spherical shell $r_t < r < 2r_t$. The black, red and cyan solid lines represent all, retained and newly associated particles, respectively. Additionally, a red dashed line shows the profile for particles identified by SUBFIND as bound to this subhalo. Right panel: The corresponding cumulative particle number profiles. The profile of newly associated particles increases as r^3 (the black dashed line) indicating a nearly uniform density from the inner subhalo region out to the surrounding environment.

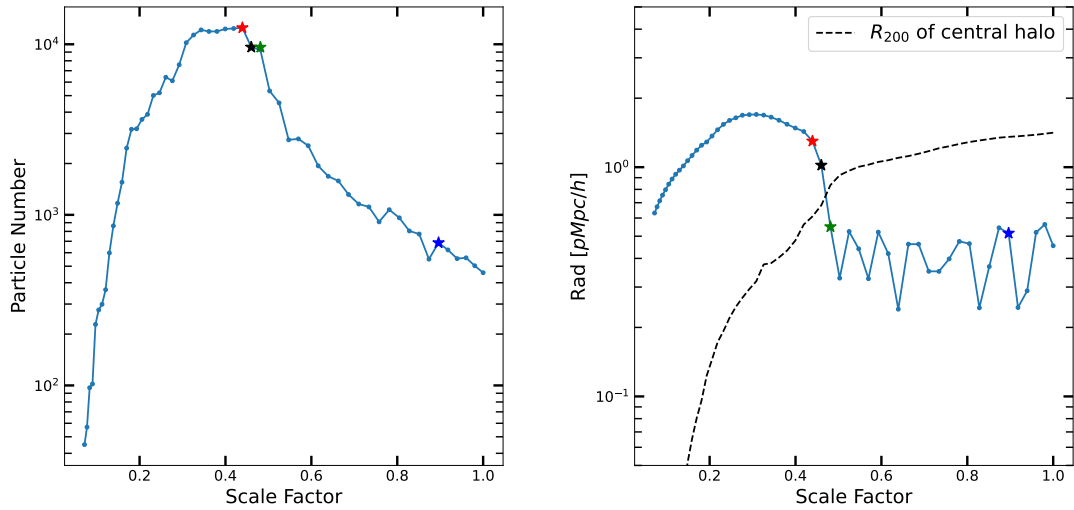


Figure 3. Evolution of subhalo mass (left panel, indicated by SUBFIND bound particle number) and of distance to host halo centre (right panel) for the subhalo of Fig.1. In both panels, the black star marks the snapshot when the subhalo is last located outside the R_{200} of host halo, which is also when set A of associated particles is defined. The red star indicates z_{max} , when r_{limit} is calculated, while the green star corresponds to z_{inf} . We also marked $z = 0.11$ with a blue star.

$\langle n_{\text{still assoc.}} \rangle$ indicate that the fraction of the subhalo mass which has been captured after infall is still of order 10^{-4} .

These results allow us to estimate of the mass in stars that might be captured by a starless subhalo in the Milky Way’s halo. The stellar mass of the MW halo outside the Solar circle is somewhat less than $10^9 M_{\odot}$ (Deason et al. 2019). Since the dark matter mass in the relevant region is a few times $10^{11} M_{\odot}$ the ratio of stellar mass to halo mass in the material captured by an orbiting starless halo will be of order 1000. We find the total captured mass to be about 0.01% of a subhalo’s current mass, so the current stellar to dark matter mass ratio for an initially starless subhalo can be estimated as $\sim 10^{-7}$. A starless subhalo of current mass $10^7 M_{\odot}$ might thus have captured $\sim 1 M_{\odot}$ of halo stars, a $10^8 M_{\odot}$ subhalo might have captured $\sim 10 M_{\odot}$. Galactic satellites with stellar masses almost this

low have recently been identified, but it is unclear whether these are dark matter dominated (e.g. Smith et al. 2024; Tan et al. 2025; Cerny et al. 2025). All were found because they are very compact (half-light radii of a few parsecs) and very metal-poor. In the next section we study whether the captured population within an initially starless halo could plausibly be so compact and thus be identifiable against the uniform background of field stars that are just “passing through”.

3.3 The distribution of captured particles

In Figure 6 red points show distance from subhalo centre as a function of subhalo tidal radius for all newly captured particles (i.e. those members of $B_i \setminus A_i$ that are bound to subhalo i at $z = 0.11$) for

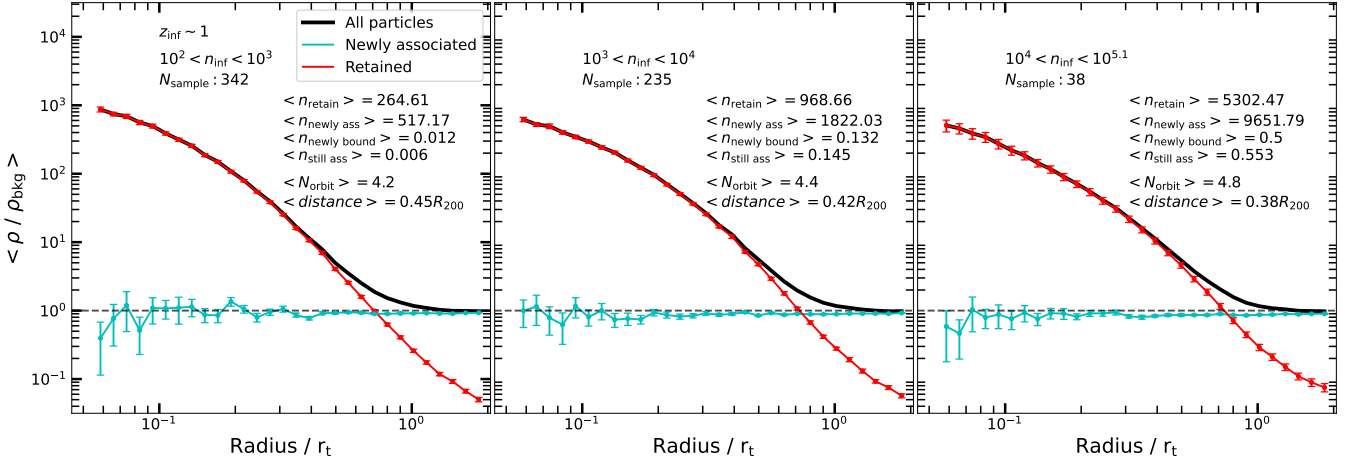


Figure 4. Stacks of spherically averaged normalized density profiles at $z = 0.11$ similar to those shown for an individual subhalo in Fig.2. The black, red and cyan solid lines represent straight averages for all, for retained and for newly associated particles, respectively. Error bars give the standard error in the mean estimated from the scatter among the profiles. From left to right, the panels show stacks for different ranges of n_{inf} . Additional legends give the number of profiles in each stack, the mean numbers of retained and newly associated particles, the mean number of newly associated particles which are also bound (according to SUBIND), and the mean number of newly associated particles which are still associated at $z = 0$. Two final legends give the mean number of orbits executed by $z = 0.11$ and the mean halocentric distance of the subhaloes at this time.

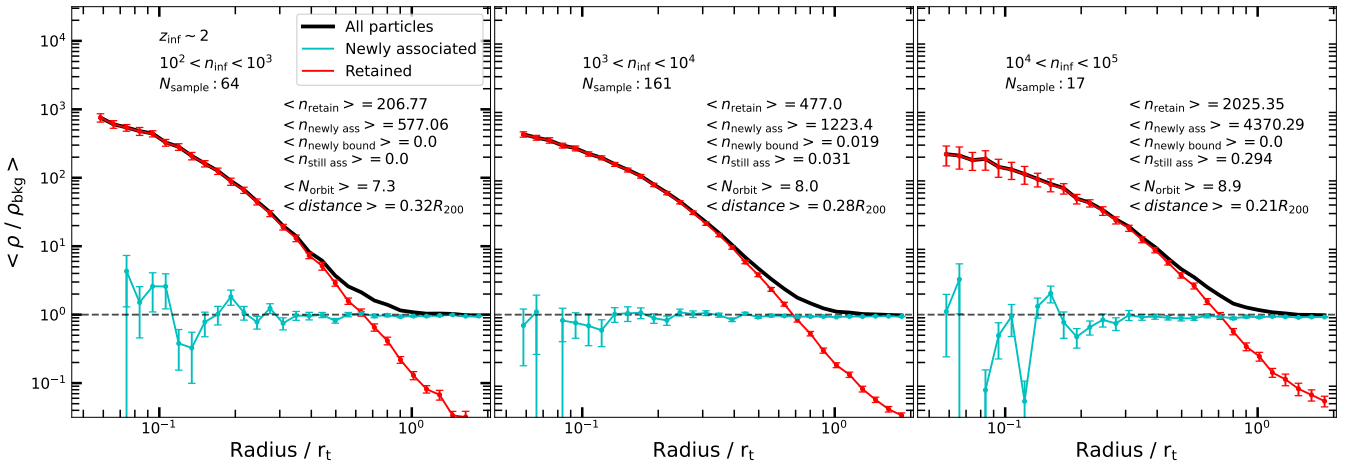


Figure 5. As Fig 4, but for $z_{\text{inf}} \approx 2$

all the subhaloes in Figures 4 and 5. Black points show the median distance of retained particles for these same subhaloes. This median distance is typically about $r_t/4$, as shown by the black line. The great majority of newly captured particles lie above this line with median distance closer to r_t (the mustard line). Our definition of retained and newly associated particles requires them to lie within $2r_t$ (the blue line); since newly associated particles are almost uniformly distributed within this radius, their median distance is $2^{2/3}r_t$. Most newly captured particles are significantly closer to subhalo centre than this, but as a population they are substantially less centrally concentrated than retained particles. Objects like Ursa Major III (Smith et al. 2024) cannot be made of captured stars, since their characteristic property is that they are much *more* concentrated than the dark haloes they live in (if indeed they have one).

The positions and velocities of originally starless haloes are, by definition, unknown, and these results show that they cannot be found

using the positions of the $\sim 0.01\%$ of their newly associated stars which are actually captured. One might wonder if sufficiently accurate kinematic data would allow them to be found through clustering in velocity space. Figure 7 shows that unfortunately this is not the case. Here we plot two components of the velocity in the rest-frame of the main halo for all particles at $z = 0.11$ that are newly associated with the particular subhalo of Figures 1, 2 and 3. The red circle indicates the subhalo velocity and has radius equal to its escape velocity. While the spatial distribution of newly associated stars is uniform and featureless within $2r_t$, the velocity distribution shows a remarkably rich structure including tight knots corresponding to kinematically cold streams of dark matter passing through the subhalo. No velocity-space feature is associated with the subhalo itself, as could have been anticipated from the fact that this particular subhalo had no newly captured particles.

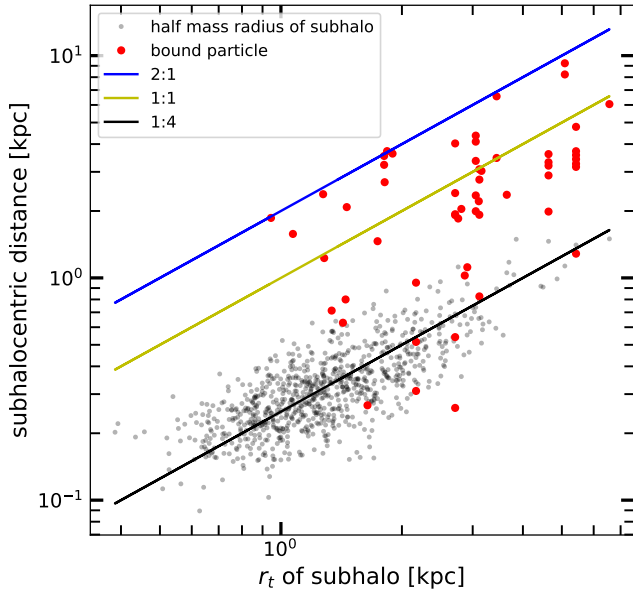


Figure 6. Black points plot the half-mass radius of retained particles against tidal radius for each subhalo in the samples of Figures 4 and 5. Red points plot the distance of newly captured particles from subhalo centre against subhalo tidal radius. We reduce all lengths by a factor of 10 to rescale our Phoenix haloes to the halo mass of Milky Way-like galaxies ($\sim 10^{12} M_{\odot}$).

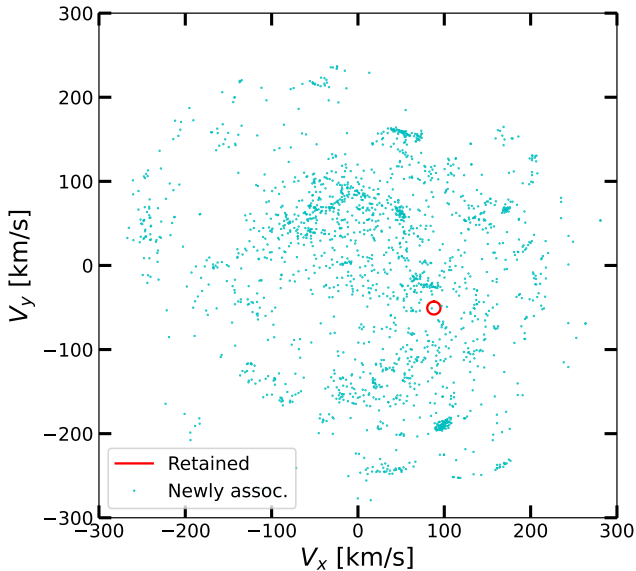


Figure 7. Velocities relative to the main halo centre-of-mass for newly associated particles at $z = 0.11$ within the subhalo shown in Figures 1, 2 and 3. The velocities are scaled down by a factor of 10 to correspond to a halo of mass $\sim 10^{12} M_{\odot}$ similar to that of the Milky Way. The red circle is located at the velocity of the subhalo itself and has a radius which encloses all particles bound to it. Note the structure in the distribution of newly associated particles which includes several dense clumps corresponding to kinematically cold dark matter streams unassociated with this particular subhalo.

4 DISCUSSION

The principal result of our analysis is that the capture of dark matter particles or stars by orbiting dark matter subhaloes is rare but does occur. For subhaloes which have completed at least three or four orbits within their host, the fraction of their bound mass acquired since infall is about one part in 10,000, and does not appear to depend strongly on subhalo mass or on halo residence time. We have checked and find that roughly half of these captured particles were within twice the limiting radius we defined for identifying particles with the subhalo at infall (i.e. within $4R_{200}(z_{\max})$). Thus much of the captured material was plausibly part of a stream associated with the infalling halo, and so plausibly has few stars. Captured stars would have to have been formed at the centre of a different early halo which was subsequently tidally disrupted. Thus, the star to dark matter mass ratio of the captured material is likely to be smaller than that of the host halo as a whole.

As would intuitively be expected, newly captured material is typically less strongly bound to a subhalo than material that has been retained since infall, and so is less strongly concentrated towards subhalo centre. As a result, there is no detectable density contrast relative to the very much larger and effectively spatially uniform background of halo material that is just passing through the subhalo on unbound orbits. This material is almost all moving at relative velocities much larger than the escape velocity from the subhalo, but it has substantial structure in velocity space which precludes detection of the captured component unless the precise velocity of the subhalo is already known. Thus, initially starless subhaloes could not be detected through velocity space clumping of halo stars.

Our primary analysis has assumed that the results we have obtained for the Phoenix suite of cluster simulations can be applied (after scaling down by a factor of ten in size and velocity) to haloes of galaxies like the Milky Way. Gao et al. (2012) compare many properties of the Phoenix haloes to the 1,000 times less massive haloes of the Aquarius suite (Springel et al. 2008). They find that the difference in mass manifests primarily in lower concentrations and formation times and in larger amounts of substructure in the Phoenix haloes. The shifts are relatively modest and should not significantly affect results for subhaloes of given (relative) mass and infall time. We have verified this (and also the lack of any significant resolution dependence in our primary results) by analysing the two highest resolution simulations of the Aquarius-A halo; details are given in the Appendix.

Our results indicate that initially starless subhaloes will capture too few field stars to be distinguished against the much larger background of stars that are just passing through on almost unperturbed orbits. Because of the near-perfect scaling of these dynamical processes with halo mass, initially starless dark matter clumps in even smaller objects (for example, subhaloes in the haloes of dwarf satellite galaxies) will be even more difficult to detect, rarely capturing even a single star from the ambient population. Unfortunately, stellar capture is not a viable route for detecting initially starless dark matter clumps in any known system.

ACKNOWLEDGEMENTS

We are grateful to Volker Springel for reprocessing the Aquarius simulations and helpful discussions. We thank the Aquarius and Phoenix collaborations for permission to use the simulations on which the results of this paper are based. HY and LG acknowledge support from the National Natural Science Foundation of China (Grant No. 12588202) and the National Key Research and Development Program of China (Grant No. 2023YFB3002500). In addition,

HY thanks LACEGAL project with European Union's HORIZON-MSCA-2021-SE-01 Research and Innovation program under the Marie Skłodowska-Curie grant agreement No. 101086388 for the grant which made possible the stay in Germany during which much of this work was carried out.

DATA AVAILABILITY

The simulation data used in this article will be shared upon reasonable request to the corresponding author.

REFERENCES

- Benitez-Llambay A., Frenk C., 2020, *MNRAS*, **498**, 4887
 Bertone G., Hooper D., Silk J., 2005, *Phys. Rep.*, **405**, 279
 Bond J. R., Cole S., Efstathiou G., Kaiser N., 1991, *ApJ*, **379**, 440
 Borrow J., Kannan R., Garaldi E., Smith A., Vogelsberger M., Pakmor R., Springel V., Hernquist L., 2023, *MNRAS*, **525**, 5932
 Cerny W., et al., 2025, *arXiv e-prints*, p. [arXiv:2510.02431](https://arxiv.org/abs/2510.02431)
 Davis M., Efstathiou G., Frenk C. S., White S. D. M., 1985, *ApJ*, **292**, 371
 Deason A. J., Belokurov V., Sanders J. L., 2019, *MNRAS*, **490**, 3426
 Efstathiou G., 1992, *MNRAS*, **256**, 43P
 Gao L., White S. D. M., Jenkins A., Stoehr F., Springel V., 2004, *MNRAS*, **355**, 819
 Gao L., Navarro J. F., Frenk C. S., Jenkins A., Springel V., White S. D. M., 2012, *MNRAS*, **425**, 2169
 Guo Q., White S., Li C., Boylan-Kolchin M., 2010, *MNRAS*, **404**, 1111
 Gutcke T. A., Pfrommer C., Bryan G. L., Pakmor R., Springel V., Naab T., 2022, *ApJ*, **941**, 120
 Jenkins A., Frenk C. S., White S. D. M., Colberg J. M., Cole S., Evrard A. E., Couchman H. M. P., Yoshida N., 2001, *MNRAS*, **321**, 372
 Klypin A., Kravtsov A. V., Valenzuela O., Prada F., 1999, *ApJ*, **522**, 82
 Moore B., Governato F., Quinn T., Stadel J., Lake G., 1998, *ApJ*, **499**, L5
 Okamoto T., Gao L., Theuns T., 2008, *MNRAS*, **390**, 920
 Peñarrubia J., Errani R., Walker M. G., Gieles M., Boekholt T. C. N., 2024, *MNRAS*, **533**, 3263
 Press W. H., Schechter P., 1974, *ApJ*, **187**, 425
 Sawala T., et al., 2015, *MNRAS*, **448**, 2941
 Sheth R. K., Tormen G., 1999, *MNRAS*, **308**, 119
 Smith S. E. T., et al., 2024, *ApJ*, **961**, 92
 Spergel D. N., et al., 2003, *ApJS*, **148**, 175
 Springel V., White S. D. M., Tormen G., Kauffmann G., 2001, *MNRAS*, **328**, 726
 Springel V., et al., 2005, *Nature*, **435**, 629
 Springel V., et al., 2008, *MNRAS*, **391**, 1685
 Tan C. Y., et al., 2025, *arXiv e-prints*, p. [arXiv:2510.11684](https://arxiv.org/abs/2510.11684)
 Tormen G., Diaferio A., Syer D., 1998, *MNRAS*, **299**, 728
 Wang J., Bose S., Frenk C. S., Gao L., Jenkins A., Springel V., White S. D. M., 2020, *Nature*, **585**, 39
 Wang C.-W., Cooper A. P., Bose S., Frenk C. S., Hellwing W. A., 2023, *ApJ*, **958**, 166
 White S. D. M., Rees M. J., 1978, *MNRAS*, **183**, 341
 Xie L., Gao L., 2015, *MNRAS*, **454**, 1697
 Zheng H., Bose S., Frenk C. S., Gao L., Jenkins A., Liao S., Liu Y., Wang J., 2024, *MNRAS*, **528**, 7300
 Zhu B., Gao L., 2024, *arXiv e-prints*, p. [arXiv:2410.16176](https://arxiv.org/abs/2410.16176)

APPENDIX: TESTS OF RESOLUTION AND HALO MASS SCALING USING AQUARIUS HALOES

In this appendix we use two simulations from the Aquarius suite (Springel et al. 2008) to test how our results depend on halo mass and on simulation resolution. Aq-A-2 is an isolated halo of mass, $M_{200c} =$

$1.8 \times 10^{12} M_{\odot}$. It was simulated with a similar zoom set-up and a similar number of particles to the Phoenix haloes analysed in the main text. This particular halo has a quiet history with an early formation time ($z_{\text{form}} = 1.9$, defined as the redshift when M_{200c} of the main progenitor is half the final value) and a high concentration ($c_{200c} = 16$) particularly when compared with the much more massive cluster haloes of the Phoenix suite (for which the median values of z_{form} and c_{200c} are 0.5 and 4.9, respectively). Aq-A-1 is a simulation of the same halo with 8 times higher mass resolution; Springel et al. (2008) show that most halo and subhalo properties are very well converged between these two simulations.

We have repeated the analysis which led to Figures 4 and 5 for these two simulations and we present the results in figures 8 and 9. Because of the higher concentration and earlier formation time of the Aquarius halo its subhalo population is shifted to substantially lower (relative) masses than in the Phoenix simulations. As a result, only the two lower ranges of n_{inf} are populated in Aq-A-2. The higher mass resolution of Aq-A-1 results in all 3 ranges being populated, but the subhalo infall masses corresponding to the range limits are now 8 times lower.

Both qualitatively and quantitatively, the results for these Aquarius haloes are very similar to those shown in the main text for the Phoenix haloes. Despite the large differences in halo mass, formation time and concentration, newly associated particles are uniformly distributed across each subhalo and are almost all unbound. The fraction of subhalo mass that is truly captured is unchanged, about 10^{-4} both for $z \sim 2$ and for $z \sim 1$, again with no obvious dependence on subhalo mass. The only clear systematic difference with the Phoenix case is that surviving subhaloes in Aquarius-A have, on average, completed fewer orbits since infall than in Phoenix. Results are well converged between Aq-A-2 and Aq-A-1 showing that particle discreteness has no substantial effect on our results. Thus it appears that the principal results of this paper are almost independent of halo mass and concentration and so can be safely extrapolated over the full range of halo masses.

This paper has been typeset from a \LaTeX file prepared by the author.

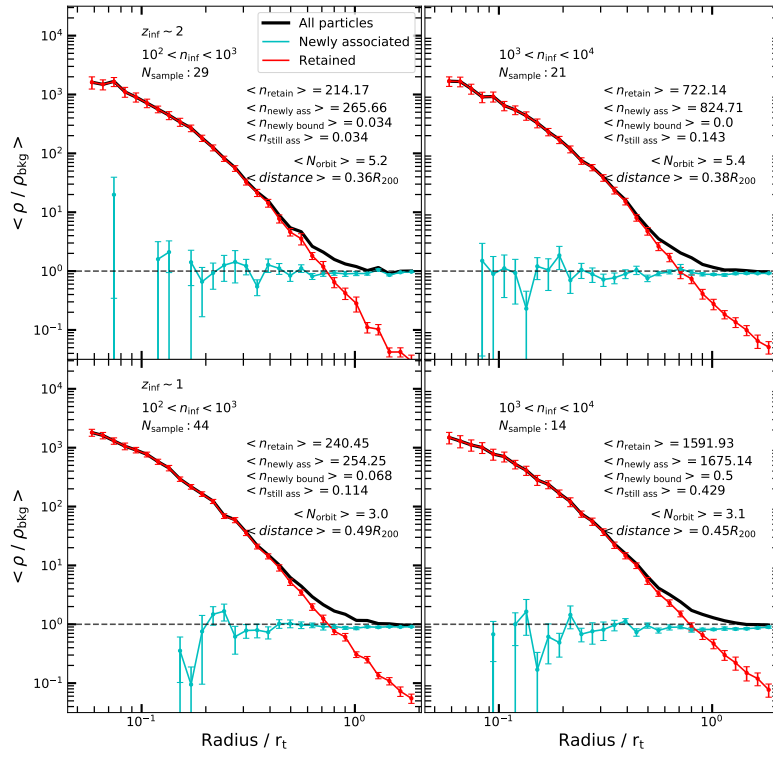


Figure 8. Same as Fig 4, with all definitions and legends unchanged, but for the Aq-A-2 simulation. From top to bottom, the panels show results at $z_{\text{inf}} \approx 1$ and $z_{\text{inf}} \approx 2$, respectively.

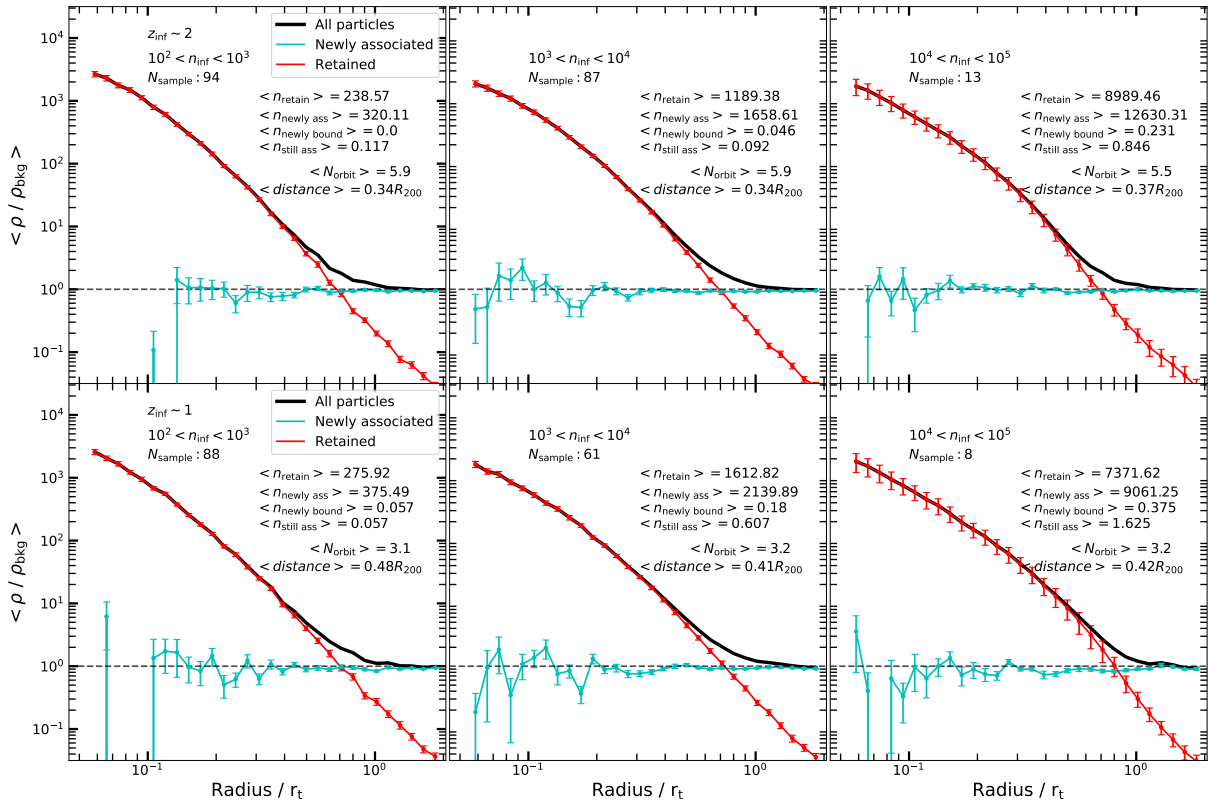


Figure 9. Same as Fig 8, but for the Aq-A-1 simulation.